Proceedings of ICFDP8:
8th Int. Congress of Fluid Dynamics & Propulsion
December 14-17,2006,Sharm El Shiekh, Sinai, Egypt.

ICFDP8-EG-141

EVALUATION OF TURBULENCE MODELS FOR FLOW OVER A FINNED HIGH SPEED TRAIN

I. K. Mohamed
Higher Institute of Energy
South Valley University, Aswan, Egypt.

M.A.Serag-Eldin
Mechanical Engineering Department
American University in Cairo, Cairo, Egypt.

A.S.Sabry
Mechanical Engineering Department
Cairo University, Cairo, Egypt.

Y.P.Kohama
Institute of Fluid Science, Tohoku University, Sendai, Japan.

ABSTRACT

The present paper evaluates seven different mathematical models for the prediction of the flow over high speed trains. All models incorporate the three-dimensional form of the mass conservation and momentum equations, however they differ in the turbulence model adopted. An unstructured grid is used which fits the boundary geometry very closely and allows grid refinement in critical regions.

Each model is evaluated against corresponding experimental measurements for a scaled down version of a finned high speed train displaying front and rear end longitudinal fins. The results obtained from all turbulence models are remarkably close, although they range widely in complexity. The agreement with measurements is generally very good, except in regions affected by trailing edge vortices. The Realizable k-ε model was found to yield the closest value of the coefficient of drag, although other models seemed to yield better agreement with the measured velocity field in many regions of the flow.

INTRODUCTION

High speed trains reach speeds of 300 km/hr and above. At 300 km/hr, a train can use up to 90% of the traction power available at the wheels to overcome aerodynamic drag, King et al (1993). Thus it is imperative to design such trains to offer minimum resistance to the surrounding air flow.

Because most high speed trains run in both directions, the nose and rear end shapes are usually identical In addition to streamlining, the introduction of longitudinal fins in the fore and front sections may help reduce trailing edge wakes, a major contributor to aero-dynamic drag. The design of such trains could benefit greatly from the use of efficient and accurate computational software.

Therefore the main objective of the present research is to present and assess a suitable mathematical model which can serve as a reliable and efficient design tool. To reach this objective, the performance of seven different turbulence models is investigated, which range in sophistication from a one dimensional model of turbulence to the Reynolds stress model. This is done by comparing the associated numerical predictions against corresponding experimental measurements, conducted on a scaled down model of a finned high speed train.

First, the considered train geometry is described. The investigated mathematical models are then introduced. Numerical predictions from each model are compared together and against corresponding measurements, and the results are duly discussed. Finally a summary and conclusion is presented.

NOMENCLATURE

A_0 ,A_s	RKE turbulence model contants
E	total energy/unit mass
G	rate of generation term
k	turbulence kinetic energy
M	Mach number
q	total heat flux
S	source terms
u,v,w	components of V in x,y,z directions.

x,y,z	Cartesian coordinates directions
V	velocity vector
$\forall$	volume of cell

Greek letters

ε	rate of dissipation of k
μ	viscosity
ν	kinematic viscosity
ρ	fluid density
σ	Prandtl number
τ	viscous stress tensor

TRAIN GEOMETRY

The train geometry considered in the present investigations features identical nose and trailing end shapes, connected by a continuous straight tube of uniform cross-section, representing main train body. For economy of calculations, the adopted tube length is much shorter than that in a real train; however, the extra length is not expected to introduce new features in the investigated flow. This practice is also very common in experimental investigations.

Figure 1 reveals the train geometry that will be employed in the present investigations; the nose and rear ends are similar to the Japanese Shinkansen series 300. The dimensions are in millimeters and correspond to a scaled down model for which experimental measurements are available, Mohamed(2006). The train height is 110 m.m.

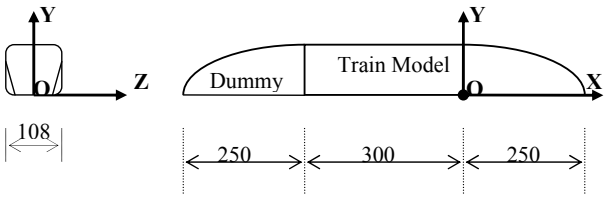

Figure 1. Train geometry employed for investigations.

Figure 2 shows a picture of the train model displaying clearly the longitudinal fins on either side of the train nose.

Figure 2. Picture of train model displaying longitudinal fins.

MATHEMATICAL MODEL

Governing Equations

The governing equations, cast in integral Cartesian coordinates for an arbitrary control volume $\forall$ with differential surface area dA, may all be cast in the following general form:

$$\frac{\partial}{\partial t}\int_{\forall} W\, d\forall + \oint [F - G].dA = \int_{\forall} H\, d\forall \qquad (1)$$

Where the vectors W, F and G are defined as the vectors:

$$W = \begin{Bmatrix} \rho \\ \rho u \\ \rho v \\ \rho w \\ \rho E \end{Bmatrix},\ F = \begin{Bmatrix} \rho V \\ \rho V u + p\hat{i} \\ \rho V v + p\hat{j} \\ \rho V w + p\hat{k} \\ \rho V E + pV \end{Bmatrix},\ G = \begin{Bmatrix} 0 \\ \tau_{xi} \\ \tau_{yi} \\ \tau_{zi} \\ \tau_{ij} v_j + q \end{Bmatrix} \qquad (2)$$

and the vector H contains source terms such as body forces and energy sources.Here ρ, V, E, and p are the density, velocity vector, total energy per unit mass, and pressure of the fluid, respectively. τ is the viscous stress tensor, and q is the heat flux.

Turbulence Models

In order to render the computations tractable, the instantaneous time-dependent equations(1,2) are time averaged, and a turbulence model is employed to procure closure of equations. This results in the disappearance of the time-derivative term, and the replacement of the viscous stresses with effective turbulence stresses. The turbulence models considered here are:

i) **The Spalart-Allmaras model (SA)**

The SA model, Bardina , Huang and Coakley(1997), is a relatively simple one equation model that solves a transport equation for a quantity $\tilde{\nu}$ which is identical to the turbulent kinematic viscosity except in the near-wall (viscous-affected) region. The transport equation for $\tilde{\nu}$ is:

$$\frac{\partial}{\partial t}(\rho\tilde{\nu}) + \frac{\partial}{\partial x_i}(\rho\tilde{\nu}u_i) = G_\nu + \frac{1}{\sigma_{\tilde{\nu}}}\left[\frac{\partial}{\partial x_j}\left\{(\mu+\rho\tilde{\nu})\frac{\partial\tilde{\nu}}{\partial x_j}\right\} + C_{b2}\rho\left(\frac{\partial\tilde{\nu}}{\partial x_j}\right)^2\right] - Y_\nu \qquad (3)$$

where G_ν is the production of turbulent viscosity and Y_ν is the destruction of turbulent viscosity that occurs in the near-wall region due to wall blocking and viscous damping. $\sigma_{\tilde{\nu}}$ and C_{b2} are constants and ν is the molecular kinematic viscosity. The turbulent viscosity, μ_t is computed from:

$$\mu_t = \rho\tilde{\nu} f_{\nu 1} \qquad (4)$$

where $f_{\nu 1}$ is a viscous damping function.

ii) **The standard k-ε model (SKE)**

The SKE model, Launder and Spalding(1974), requires the solution of transport equations for the kinetic energy of turbulence k, and its rate of dissipation, ε. The equation for k was derived from the exact equation, while that of ε was obtained using physical reasoning and bears little resemblance to its mathematically exact counterpart.

In the derivation of the model, it was assumed that the flow is fully turbulent, and the effects of molecular viscosity

are negligible. The SKE model is therefore valid only for fully turbulent flows.

The transport equations for k, and ε are:

$$\frac{\partial}{\partial t}(\rho k)+\frac{\partial}{\partial x_i}(\rho k u_i)=\frac{\partial}{\partial x_j}\left[\left(\mu+\frac{\mu_t}{\sigma_k}\right)\frac{\partial k}{\partial x_j}\right]+G_k+G_b-\rho\varepsilon-Y_M \quad (5)$$

and

$$\frac{\partial}{\partial t}(\rho\varepsilon)+\frac{\partial}{\partial x_i}(\rho\varepsilon u_i)=\frac{\partial}{\partial x_j}\left[\left(\mu+\frac{\mu_t}{\sigma_\varepsilon}\right)\frac{\partial\varepsilon}{\partial x_j}\right]+C_{1\varepsilon}\frac{\varepsilon}{k}(G_k+C_{3\varepsilon}G_b)-C_{2\varepsilon}\rho\frac{\varepsilon^2}{k} \quad (6)$$

In these equations, G_k represents the generation of turbulence kinetic energy due to the mean velocity gradients; G_b is the generation of turbulence kinetic energy due to buoyancy; Y_M represents the contribution of the fluctuating dilatation in compressible turbulence to the overall dissipation rate. $C_{1\varepsilon}$, $C_{2\varepsilon}$ and $C_{3\varepsilon}$ are constants. σ_k and σ_ε are the turbulent Prandtl numbers for k and ε, respectively.

The turbulent (or eddy) viscosity, μ_t, is computed by combining k and ε as follows:

$$\mu_t = \rho C_\mu \frac{k^2}{\varepsilon} \quad (7)$$

where C_μ=.09 is a model constant. The other model constants $C_{1\varepsilon}$, $C_{2\varepsilon}$, σ_k and σ_ε acquire the following universal values :

$$C_{1\varepsilon}=1.44,\ C_{2\varepsilon}=1.92,\ C_\mu=0.09,\ \sigma_k=1.0,\ \sigma_\varepsilon=1.3 \quad (8)$$

iii) **The renormalized group k-ε model (RNGKE)**

The RNG-based k-ε turbulence model is derived from the instantaneous Navier-Stokes equations, using a mathematical technique called "renormalization group" methods. This results in constants different from those in the standard k-ε model, and additional terms and functions in the transport equations for k and ε, Yakhot and Orszag(1986), Yakhot and Smith(1992), and Nagano and Itazu(1997).

.

The RNGKE model transport equations for k and ε are:

$$\frac{\partial}{\partial t}(\rho k)+\frac{\partial}{\partial x_i}(\rho k u_i)=\frac{\partial}{\partial x_j}\left(\alpha_k\mu_{eff}\frac{\partial k}{\partial x_j}\right)+G_k+G_b-\rho\varepsilon-Y_M \quad (9)$$

and

$$\frac{\partial}{\partial t}(\rho\varepsilon)+\frac{\partial}{\partial x_i}(\rho\varepsilon u_i)=\frac{\partial}{\partial x_j}\left(\alpha_\varepsilon\mu_{eff}\frac{\partial\varepsilon}{\partial x_j}\right)+C_{1\varepsilon}\frac{\varepsilon}{k}(G_k+C_{3\varepsilon}G_b)-C_{2\varepsilon}\rho\frac{\varepsilon^2}{k}-R_\varepsilon \quad (10)$$

Here G_k represents the rate of generation of turbulence kinetic energy due to the mean velocity gradients; G_b is the generation of turbulence kinetic energy due to buoyancy; Y_M represents the contribution of the fluctuating dilatation in compressible turbulence to the overall dissipation rate. The quantities α_k and α_ε are the inverse effective Prandtl numbers for k and ε, respectively.

The scale elimination procedure in RNGKE theory results in a differential equation for turbulent viscosity:

$$d\left(\frac{\rho^2 k}{\sqrt{\varepsilon\mu}}\right)=1.72\,\frac{\tilde{\nu}}{\sqrt{\tilde{\nu}^3-1+C_\nu}}\,d\tilde{\nu} \quad (11)$$

where

$$\tilde{\nu}=\mu_{eff}/\mu, \qquad C_\nu\approx 100 \quad (12)$$

In the high-Reynolds-number limit,

$$\mu_t = \rho C_\mu \frac{k^2}{\varepsilon}$$

The main difference between the RNGKE and standard SKE models lies in the additional term in the ε equation :

$$R_\varepsilon = \frac{C_\mu\rho\eta^3(1-\eta/\eta_0)}{1+\beta\eta^3}\frac{\varepsilon^2}{k} \quad (13)$$

where

$$\eta\equiv Sk/\varepsilon, \quad \eta_0=4.38, \quad \beta=0.012 \quad (14)$$

The RNGKE model is more responsive to the effects of rapid strain and streamlines curvature than the standard k-ε model, which explains the superior performance of the RNGKE model for certain classes of flows.

The model constants $C_{1\varepsilon}$ and $C_{2\varepsilon}$ have values derived analytically by the RNGKE theory, which are 1.42 and 1.68 respectively.

iv) **The realizable k-ε model (RKE)**

The RKE model, was introduced to satisfy certain mathematical constraints on the normal stresses, Shih et al(1995). The modeled transport equations for k and ε are:

$$\frac{\partial}{\partial t}(\rho k)+\frac{\partial}{\partial x_i}(\rho k u_j)=\frac{\partial}{\partial x_i}\left(\left(\mu+\frac{\mu_t}{\sigma_k}\right)\frac{\partial k}{\partial x_j}\right)+G_k+G_b-\rho\varepsilon-Y_M \quad (15)$$

and

$$\frac{\partial}{\partial t}(\rho\varepsilon)+\frac{\partial}{\partial x_j}(\rho\varepsilon u_j)=\frac{\partial}{\partial x_j}\left[\left(\mu+\frac{\mu_t}{\sigma_\varepsilon}\right)\frac{\partial\varepsilon}{\partial x_j}\right]-\rho C_2\frac{\varepsilon^2}{k+\sqrt{\nu\varepsilon}}+C_{1\varepsilon}\frac{\varepsilon}{k}C_{3\varepsilon}G_b \quad (16)$$

In the above equations, G_k represents the generation of turbulence kinetic energy due to the mean velocity gradients; G_b is the generation of turbulence kinetic energy due to buoyancy; Y_M represents the contribution of the fluctuating dilatation in compressible turbulence to the overall dissipation rate. C_2 and $C_{1\varepsilon}$ are constants. σ_k and σ_ε are the turbulent Prandtl numbers for k and ε, respectively.

The eddy viscosity is computed from

$$\mu_t = \rho C_\mu \frac{k^2}{\varepsilon} \quad (17)$$

with C_μ computed from:

$$C_\mu \equiv \frac{1}{A_0+A_S\frac{kU^*}{\varepsilon}} \quad (18)$$

where

$$U^* \equiv \sqrt{S_{ij}S_{ij}+\tilde{\Omega}_{ij}\tilde{\Omega}_{ij}} \quad (19)$$

and

$$\tilde{\Omega}_{ij}=\Omega_{ij}-2\varepsilon_{ijk}\omega_k \ , \quad \Omega_{ij}=\overline{\Omega_{ij}}-\varepsilon_{ijk}\omega_k \quad (20)$$

where Ω_{ij} is the mean rate of rotation tensor viewed in a rotating reference frame with the angular velocity ω_k. The model constants A_0 and A_s are given by

$$A_0=4.04 \ , \qquad A_S=\sqrt{6}\cos\phi \quad (21)$$

where

$$\phi=\frac{1}{3}\cos^{-1}\left(\sqrt{6}W\right),\ W=\frac{S_{ij}S_{jk}S_{ki}}{S},\ \tilde{S}=\sqrt{S_{ij}S_{ij}},\ S_{ij}=\frac{1}{2}\left(\frac{\partial u_j}{\partial x_i}+\frac{\partial u_i}{\partial x_j}\right) \quad (22)$$

Other model constants are

$$C_{1\varepsilon}=1.44,\quad C_2=1.9,\quad \sigma_k=1.0,\quad \sigma_\varepsilon=1.2 \quad (23)$$

The term G_k, representing the production of turbulence kinetic energy, is evaluated as:

$$G_k=\mu_t S^2 \quad (24)$$

where S is the modulus of the mean rate-of-strain tensor, defined as

$$S\equiv\sqrt{2\,S_{ij}S_{ij}} \quad (25)$$

v) **The standard k-ω model (SKW)**

The SKW model, requires solution of transport equations for the turbulence kinetic energy (k) and the specific dissipation rate (ω), which can also be thought of as the ratio of ε to k, Wilcox(1998). The transport equations are the following:

$$\frac{\partial}{\partial t}(\rho k)+\frac{\partial}{\partial x_i}(\rho k u_i)=\frac{\partial}{\partial x_j}\left(\Gamma_k\frac{\partial k}{\partial x_j}\right)+G_k-Y_k \quad (26)$$

and

$$\frac{\partial}{\partial t}(\rho w)+\frac{\partial}{\partial x_i}(\rho w u_i)=\frac{\partial}{\partial x_j}\left(\Gamma_w\frac{\partial w}{\partial x_j}\right)+G_w-Y_w \quad (27)$$

In these equations, G_k represents the generation of turbulence kinetic energy due to mean velocity gradients. G_ω represents the generation of ω. Γ_k and Γ_ω represent the effective diffusivity of k and ω, respectively. Y_k and Y_ω represent the dissipation of k and ω due to compressibility.

The turbulent viscosity, μ_t, is computed from k and ω as follows:

$$\mu_t=\alpha^*\frac{\rho k}{w} \quad (28)$$

where

$$\alpha^*=\alpha^*_\infty\left(\frac{\alpha^*_0+\mathrm{Re}_t/R_k}{1+\mathrm{Re}_t/R_k}\right) \quad (29)$$

with

$$\mathrm{Re}_t=\frac{\rho k}{\mu w},\quad R_k=6,\quad \alpha^*_0=\frac{\beta_i}{3},\quad \beta_i=0.072 \quad (30)$$

Model constants are

$$\alpha^*_\infty=1.0,\ \alpha_\infty=0.52,\ \alpha_0=\frac{1}{9},\ \beta^*_\infty=0.09,\ \beta_i=0.072,\ R_\beta=8,$$
$$R_k=6,\ R_w=2.95,\ \zeta^*=1.5,\ M_{t0}=0.25,\ \sigma_k=2.0,\ \sigma_w=2.0 \quad (31)$$

vi) The shear-stress transport k-ω model (SSTKW).

In the SSTKW model, Mentor(1994), the definition of the turbulent viscosity is modified to account for the transport of the principal turbulent shear stress. Other modifications include the addition of a cross-diffusion term in the ω equation and a blending function to ensure that the model equations behave appropriately in both the near-wall and far-field zones. The transport equations are:

$$\frac{\partial}{\partial t}(\rho k)+\frac{\partial}{\partial x_i}(\rho k u_i)=\frac{\partial}{\partial x_j}\left(\Gamma_k\frac{\partial k}{\partial x_j}\right)+G_k-Y_k \quad (32)$$

and

$$\frac{\partial}{\partial t}(\rho w)+\frac{\partial}{\partial x_i}(\rho w u_i)=\frac{\partial}{\partial x_j}\left(\Gamma_w\frac{\partial w}{\partial x_j}\right)+G_w-Y_w+D_w \quad (33)$$

In these equations, G_k represents the generation of turbulence kinetic energy due to mean velocity gradients; G_ω represents the generation of ω. Γ_k and Γ_ω represent the effective diffusivity of k and ω, respectively. Y_k and Y_ω represent the dissipation of k and ω due to turbulence. D_ω represents the cross-diffusion term. The turbulent viscosity, μ_t, is computed as follows:

$$\mu_t=\frac{\rho k}{w}\frac{1}{\max\left[\frac{1}{\alpha^*},\frac{\Omega F_2}{\alpha_1 w}\right]} \quad (34)$$

where Ω_{ij} is the mean rate-of-rotation tensor, and F_1 and F_2, are blending functions. Model constants are:

$$\sigma_{k,1}=1.176,\ \sigma_{w,1}=2.0,\ \sigma_{k,2}=1.0,\ \sigma_{w,2}=1.168,\ a_1=0.31,\ \beta_{i,1}=0.075,\ \beta_{i,2}=0.0828 \quad (35)$$

vii) **The Reynolds Stress model (RSM)**

The Reynolds stress model, Sarkar and Balakrishnan (1990),Gibson and Launder(1978), Launder et al(1975) involves calculation of the individual Reynolds stresses $\overline{u_i'u_j'}$, using differential transport equations. The individual Reynolds stresses are then used to obtain closure of the Reynolds-averaged momentum equations; however modeling assumptions are still required in order to close the Reynolds stresses equations.

The exact transport equations for the transport of the Reynolds stresses, $\rho\overline{u_i'u_j'}$, may be written as follows:

$$\underbrace{\frac{\partial}{\partial t}\left(\rho\overline{u_i'u_j'}\right)}_{\text{Local Time Derivative}}+\underbrace{\frac{\partial}{\partial x_k}\left(\rho u_k\overline{u_i'u_j'}\right)}_{C_{ij}\equiv\text{Convection}}=\underbrace{-\frac{\partial}{\partial x_k}\left[\rho\overline{u_i'u_j'u_k'}+\overline{p\left(\delta_{kj}u_i'+\delta_{ik}u_j'\right)}\right]}_{D_{T,ij}\equiv\text{Turbulent Diffusion}}$$
$$+\underbrace{\frac{\partial}{\partial x_k}\left[\mu\frac{\partial}{\partial x_k}\left(\overline{u_i'u_j'}\right)\right]}_{D_{L,ij}\equiv\text{Molecular Diffusion}}-\underbrace{\rho\left(\overline{u_i'u_k'}\frac{\partial u_j}{\partial x_k}+\overline{u_j'u_k'}\frac{\partial u_i}{\partial x_k}\right)}_{P_{ij}\equiv\text{Stress Production}}-\underbrace{\rho\beta\left(g_i\overline{u_j'\theta}+g_j\overline{u_i'\theta}\right)}_{G_{ij}\equiv\text{Buoyancy Production}}$$
$$+\underbrace{\overline{p\left(\frac{\partial u_i'}{\partial x_j}+\frac{\partial u_j'}{\partial x_i}\right)}}_{\varphi_{ij}\equiv\text{Pressure Strain}}-\underbrace{2\mu\overline{\frac{\partial u_i'}{\partial x_k}\frac{\partial u_j'}{\partial x_k}}}_{\varepsilon_{ij}\equiv\text{Dissipation}}-\underbrace{2\rho\Omega_k\left(\overline{u_j'u_m'}\varepsilon_{ikm}+\overline{u_i'u_m'}\varepsilon_{jkm}\right)}_{F_{ij}\equiv\text{Production by System Rotation}} \quad (36)$$

Of the various terms in these exact equations, C_{ij}, $D_{L;ij}$, P_{ij}, and F_{ij} do not require any modeling. The terms $D_{T;ij}$, G_{ij} , Φ_{ij} , and ε_{ij} are modeled as follows:

$$D_{T,ij}=C_S\frac{\partial}{\partial x_k}\left(\rho\frac{k\overline{u_k'u_\ell'}}{\varepsilon}\frac{\partial u_i'u_j'}{\partial x_\ell}\right) \quad (37)$$

and

$$\phi_{ij}=\phi_{ij,1}+\phi_{ij,2}+\phi_{ij,\omega} \quad (38)$$

where $\Phi_{ij,1}$ is the slow pressure-strain term, also known as the return-to-isotropy term, $\Phi_{ij,2}$ is called the rapid pressure-strain term, and $\Phi_{ij,w}$ is the wall-reflection term. The slow pressure-strain term, $\Phi_{ij,1}$, is modeled as

$$\phi_{ij,1} \equiv - C_1 \rho \frac{\varepsilon}{k}\left[\overline{u_i' u_j'} - \frac{2}{3}\delta_{ij} k \right] \qquad (39)$$

with C_1 =1.8. The rapid pressure-strain term, $\Phi_{ij,2}$, is modeled as:

$$\phi_{ij,2} \equiv - C_2 \left[\left(P_{ij} + F_{ij} + G_{ij} - C_{ij} \right) - \frac{2}{3}\delta_{ij}\left(P + G - C \right) \right] \qquad (40)$$

where C_2 = 0.60, P = P_{kk}/2, G = G_{kk}/2, and C = C_{kk}/2.

The wall-reflection term, $\Phi_{ij,w}$ is modeled as

$$\phi_{ij,w} \equiv C_1' \frac{\varepsilon}{k}\left(\overline{u_k' u_m'}\, n_k n_m \delta_{ij} - \frac{3}{2}\overline{u_i' u_k'}\, n_j n_k - \frac{3}{2}\overline{u_j' u_k'}\, n_i n_k \right)\frac{k^{3/2}}{C_\ell \varepsilon d} + \qquad (41)$$

$$C_2' \left(\phi_{km,2} n_k n_m \delta_{ij} - \frac{3}{2}\phi_{ik,2} n_j n_k - \frac{3}{2}\phi_{jk,2} n_i n_k \right)\frac{k^{3/2}}{C_\ell \varepsilon d}$$

where $C_1' = 0.5$, $C_2' = 0.3$, n_k is the x_k component of the unit normal to the wall, d is the normal distance to the wall and $C_\ell = C_\mu^{3/4}/\kappa$, where C_μ = 0.09 and κ is the von Karman constant (= 0.4187).

$$\phi_{ij} = -\left(C_1 \rho\varepsilon + C_1^* P\right) b_{ij} + C_2 \rho\varepsilon \left(b_{ik} b_{kj} - \frac{1}{3} b_{mn} b_{mn} \delta_{ij} \right) + \left(C_3 - C_3^* \sqrt{b_{ij} b_{ij}} \right) \rho k S_{ij}$$

$$+ C_4 \rho k \left(b_{ik} S_{jk} + b_{jk} S_{ik} - \frac{2}{3} b_{mn} S_{mn} \delta_{ij} \right) + C_5 \rho k \left(b_{ik}\Omega_{jk} + b_{jk}\Omega_{ik} \right) \qquad (42)$$

where b_{ij} is the Reynolds-stress anisotropy tensor defined as

$$b_{ij} = -\left(\frac{-\rho \overline{u_i' u_j'} + \frac{2}{3}\rho k \delta_{ij}}{2\rho k} \right) \qquad (43)$$

The model constants are :

C_1=3.4, C_1^*=1.8, C_2=4.2, C_3=0.8, C_3^*=1.3, C_4=1.25, C_5=0.4

The dissipation tensor, ε_{ij}, is modeled as

$$\varepsilon_{ij} = \frac{2}{3}\delta_{ij}\left(\rho\varepsilon + Y_M \right) \qquad (44)$$

where $Y_M = 2\rho\varepsilon M_t^2$ is an additional "dilatation dissipation" term, and the scalar dissipation rate, ε is computed from the transport equation :

$$\frac{\partial}{\partial t}(\rho\varepsilon) + \frac{\partial}{\partial x_i}(\rho\varepsilon u_i) = \frac{\partial}{\partial x_j}\left[\left(\mu + \frac{\mu_t}{\sigma_\varepsilon} \right)\frac{\partial \varepsilon}{\partial x_j} \right] + C_{\varepsilon 1}\frac{1}{2}\left(P_{ii} + C_{\varepsilon 3} G_{ii} \right)\frac{\varepsilon}{k} - C_{\varepsilon 2}\rho\frac{\varepsilon^2}{k} \qquad (45)$$

where σ_ε = 1.0, $C_{\varepsilon 1}$ = 1.44, $C_{\varepsilon 2}$ = 1.92, $C_{\varepsilon 3}$ is evaluated as a function of the local flow direction relative to the gravitational vector.

The turbulent viscosity, μ_t, is computed similarly to the k-ε models:

$$\mu_t = \rho C_\mu \frac{k^2}{\varepsilon} \qquad (46)$$

where C_μ = 0.09.

Other models of turbulence were not considered, either because they were not well verified, too primitive, or too computationally expensive to be useful as design tools, e.g. LES and DNS models of turbulence.

Boundary Conditions and Solution

Boundary conditions are specified on all boundaries of solution domain. At inlet, the boundary values for the inlet flow velocity, inlet temperature, inlet turbulence intensity and length scale are specified. The free stream velocity is taken to be 40 m/s to correspond to the measurement conditions. The corresponding flow Reynolds number based on the train model height is 2.93 x 10^5 At outlet, the value of outlet pressure is specified; whereas gradient conditions are used for all other variables.

Solid wall boundary conditions are used for the train body. Both fixed and moving wall boundary conditions are used for the ground. Wall functions are used at all solid boundaries. .

The finite-volume-method, e.g. Versteeg and Malalasekera (1995), is employed to discretize the set of differential equations prior to solution, employing an unstructured, tetrahedral grid. Grid dependence tests were conducted with grids displaying 25989, 93845, 125811 and 158292 grid nodes, Mohamed(2006), for the various turbulence models. The results indicated an acceptably grid independent result for all models with 93845 nodes, and thus this grid was employed for the remainder of the runs.

INVESTIGATIONS

Figures(3-10) reveal corresponding measured and predicted velocity profiles, for the seven models considered.

Here X, Y and Z refer to distances in the x, y, and z Cartesian coordinates directions, respectively; measured from an origin lying at the intersection of the bottom plane of the train, the train longitudinal symmetry plane, and the upstream plane of the trailing edge section, as displayed in Figure 1. The x-direction is aligned with the longitudinal axis of the train(also free stream direction), the y-direction with the vertical, and the z-direction with the horizontal lateral direction(also horizontal cross-stream direction).

The results display the profiles at the two planes at which measurements are available from Ibrahim(2006). They comprise the train symmetry plane, Z=Z0, and another parallel plane closer to the train side walls, Z=Z30. For each plane, results are presented at both the frontal region (SF1,SF2) and the rear one (SR1,SR2). The SF1,SR1 surfaces are relatively close to the train surface, whereas the (SF2,SR2) are further out.

Figure 3 displays the projections of the local velocity vectors on the symmetry plane Z0, for the frontal region(train nose). The measured and predicted results for the seven models are displayed simultaneously; the key "V-hw"

designating hot-wire velocity measurements, whereas the keys "V-RKE", "V-RNGKE", "V-RSM", "V-SA", "V-SKE", "V-SKW", "V-SSTKW" designating results of velocity predictions employing the RKE, RNGKE, RSM, SA, SKE, SKW and SSTKW, turbulence models, respectively.

The velocity magnitudes are plotted against the x-axis, however, in this diagram and in subsequent ones, the results correspond to *variable* y-coordinates since the velocity measurements have been conducted along curved surfaces and not horizontal ones. The y-locations may however be deduced from the displayed contours of the measurement surface, SF1. Also displayed, is the contour of the train surface, T-Geom, which is convenient for reference purposes. The SF1 surface is one of the two measurement surfaces, and the one closest to the train body. The flow direction is from right to left, as suggested by the V arrow.

The profiles show a rapid dip at the tip of the train, with a quick recovery further downstream, the maximum values being adjacent to the end of the nose section. This is expected, since at the train surface, the flow must go first through a small stagnation region before accelerating over the train body, the maximum velocity being reached towards the end of the curvature.

Comparison of the predicted versus measured results, reveals generally very good agreement. The agreement between the results of the different turbulence models is also very close. The SKW model reveals the worst agreement, tending to under predict the velocity magnitude , particularly downstream the nose; so does the RKE model.

Figure 4 displays the corresponding velocity profiles at the surface SF2, which is considerably further out from the train top than surface SF1. The agreement between measurements and predictions for all models is excellent. Surprisingly the agreement with the SKW model is near perfect on this surface, and the closest among all models, although it was the poorest on the surface SW1.

Figures 5,6 display the velocity profiles at the rear end of the train, corresponding to Figures 3,4, respectively,. Figure 5 reveals that the agreement between measurements and predictions is generally quite good for all models, except very close to the trailing edge, where all models under predict the wake deficit. The best in this region is the RNGKE and RSM models, although other models are superior upstream. However, it is encouraging to see that the trends are captured quite closely by all models.

Figure 6 reveals that further out from the train top, the results of all models are in close agreement with measurements.

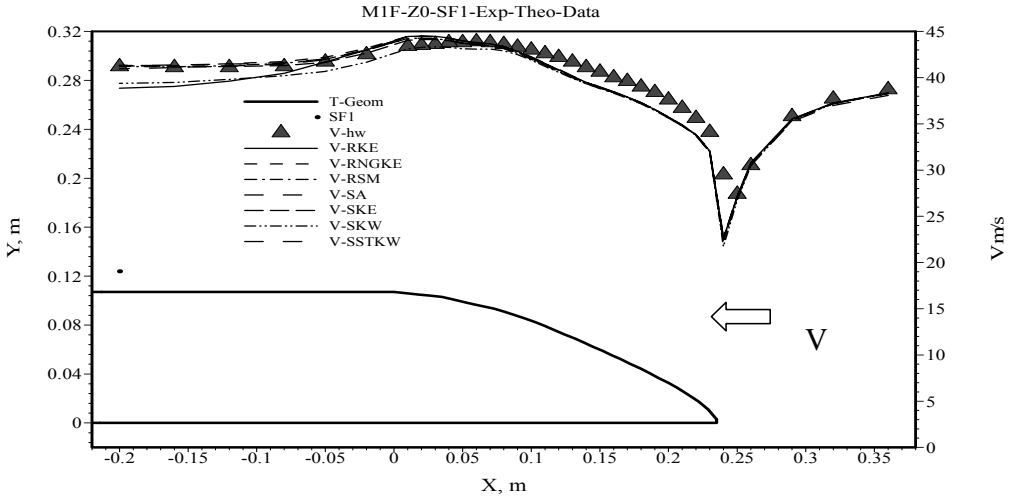

Figure 3. Velocity Profiles at Front-end of train symmetry plane, measurement surface SF1

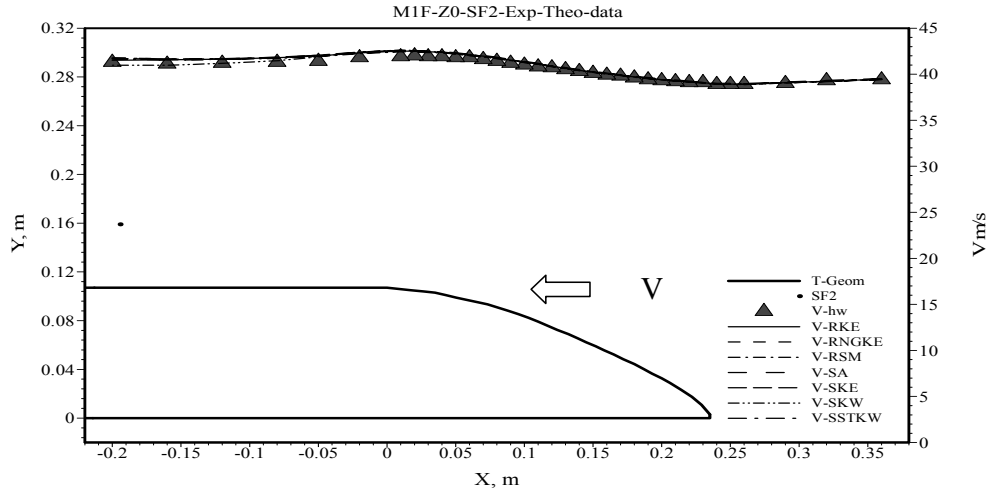

Figure 4. Velocity Profiles at Front-end of train symmetry plane, measurement surface SF2.

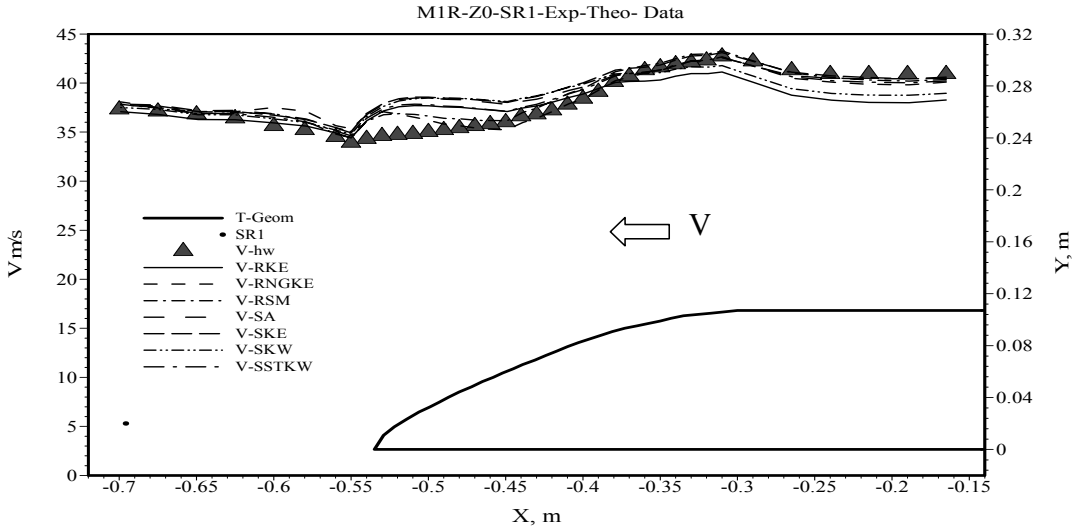

Figure 5. Velocity Profiles at Rear-end of train symmetry plane, measurement surface SR1.

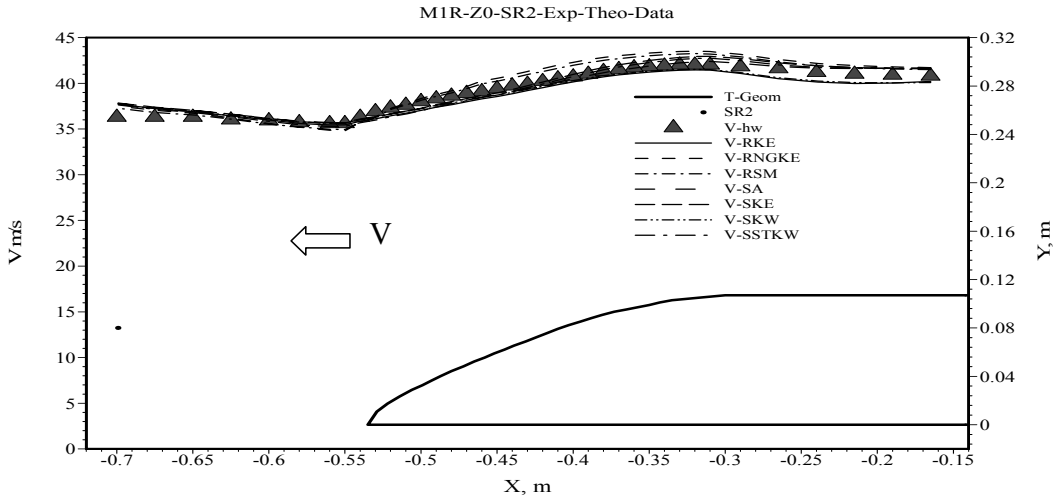

Figure 6. Velocity Profiles at Rear-end of train symmetry plane, measurement surface SR2.

Figures 7,8,9,10 display the corresponding velocity profiles at the near edge plane Z30. Figure 7 displays the front end results at the measurement surface SF1, which is very close to the train top surface. Again all the model predictions display close agreement with each other, and generally good agreement with measurements, except at the leading edge front, where they over predict the spike/drop in velocity. However, due to the extreme proximity of the measurement surface to the leading edge, and due to the very rapid changes occurring there, the disagreement between measurements and predictions could be caused in part, due to interpolation and location errors.

Figure 8 displays the front end velocity profiles at the measurement surface SF2, which is displaced a considerable distance from train surface. The agreement between all models and measurements is excellent.

Figure 9 reveals the rear end velocity profiles along the measurement surface SR1, which is somewhat close to the train surface. The agreement is good away from the trailing edge; however close to it, all the predicted results fail to predict a measured spike. Visualization techniques, Ibrahim(2006), revealed the flow in this region to be highly three-dimensional, unsteady and turbulent, with continuous generation of trailing edge vortices. Figure 10 reveals the corresponding profiles further out, i.e. at measurement surface SR2. The agreement between measurements and predictions is slightly better, but considerable deviations are still present near the sharp trailing edge.

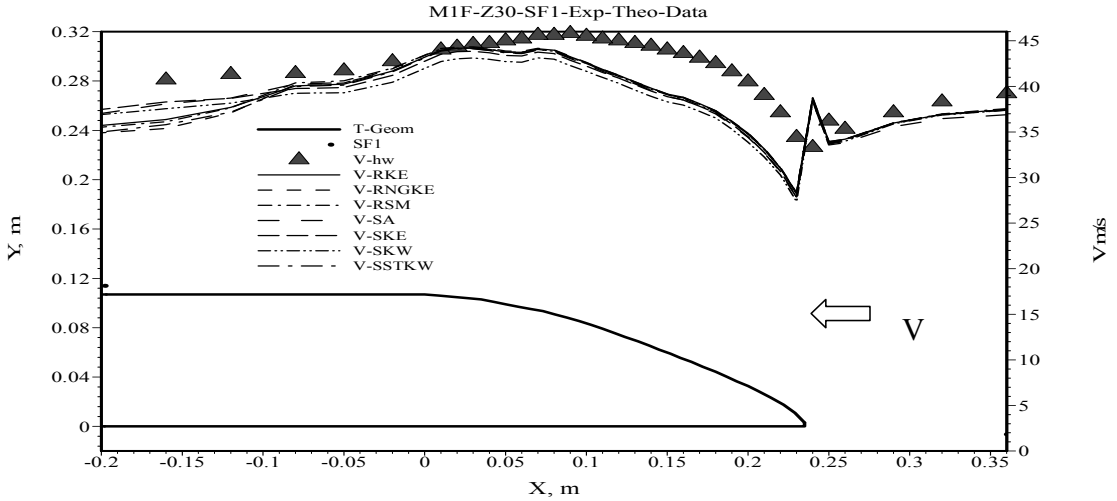

Figure 7. Velocity Profiles at Front-end of train near edge plane Z30, measurement surface SF1

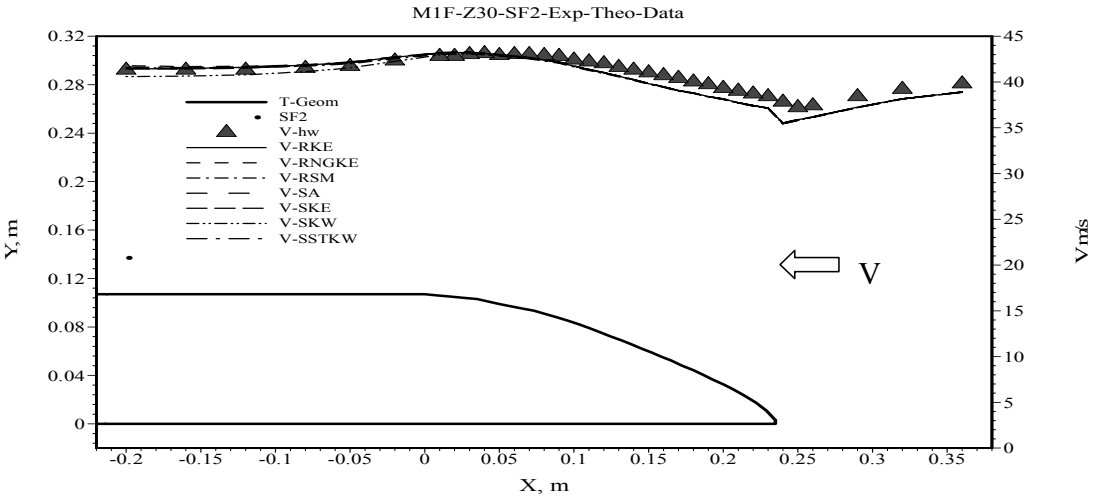

Figure 8. Velocity Profiles at Front-end of train near edge plane Z30, measurement surface SF2

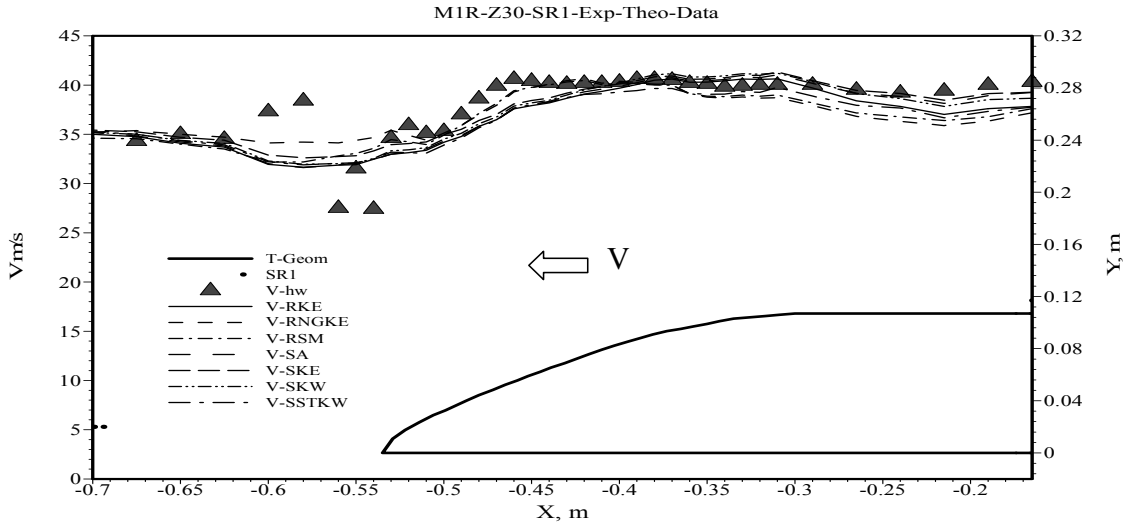

Figure 9. Velocity Profiles at rear-end of train, near edge plane Z30, measurement surface SR1

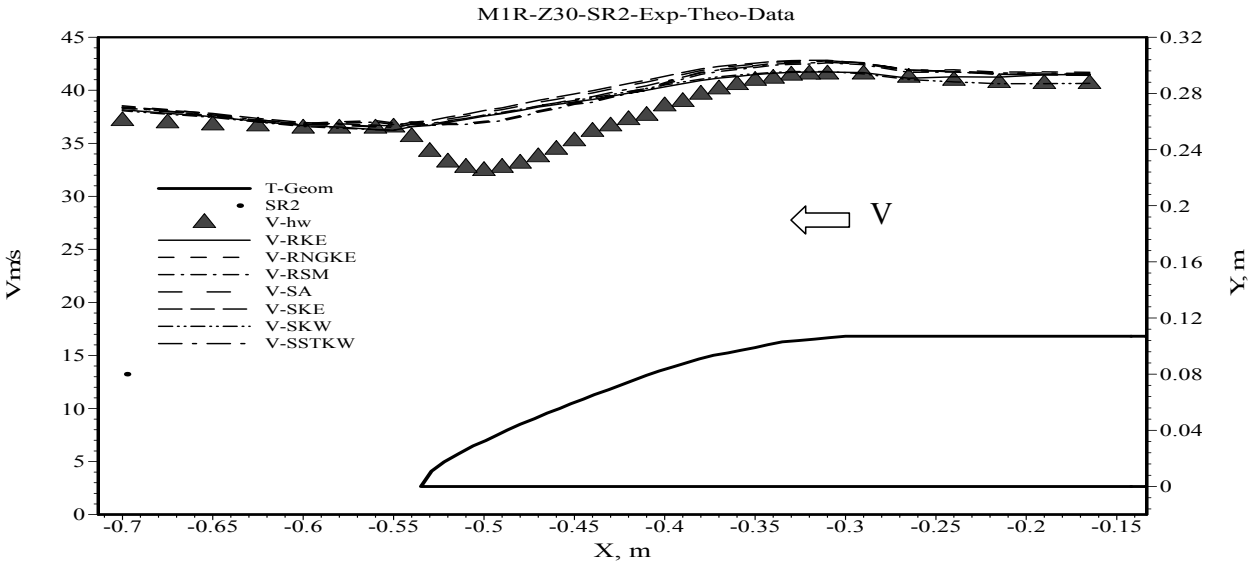

Figure 10. Velocity Profiles at rear-end of train, near edge plane Z30, measurement surface SR2.

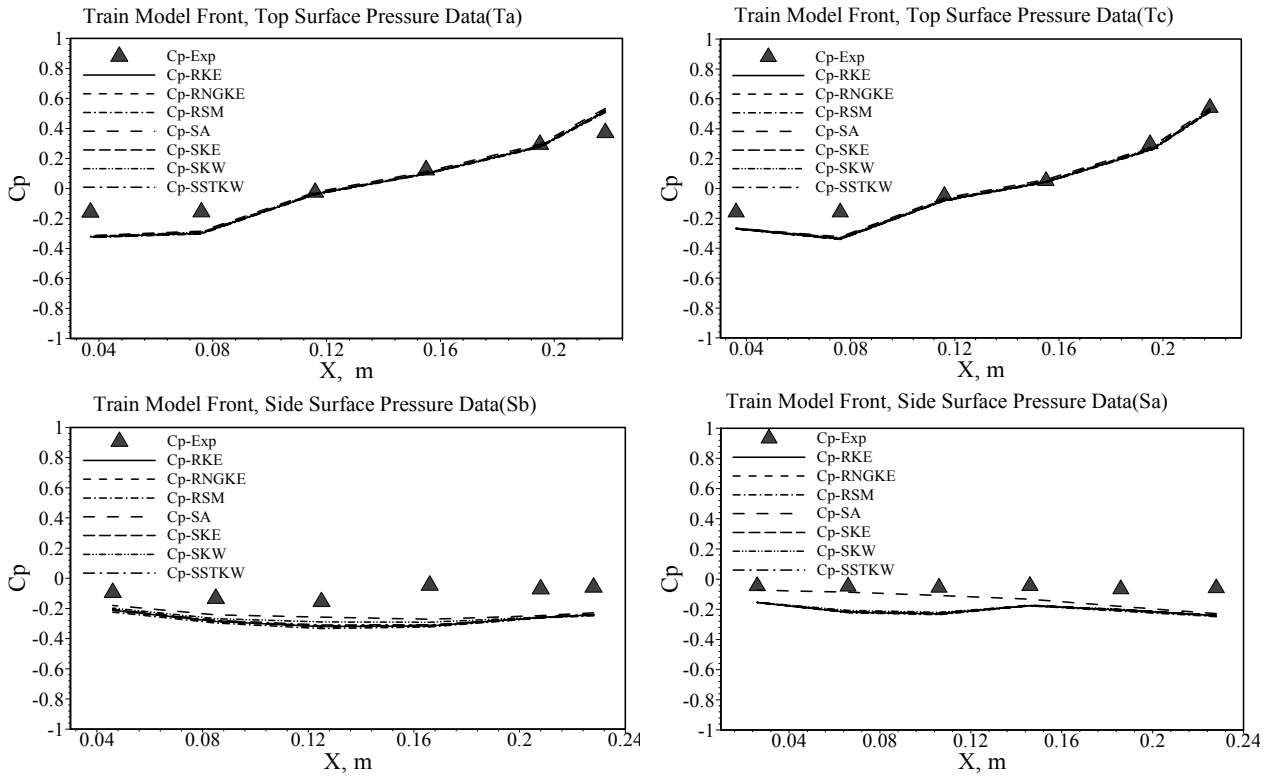

Figure 11. Measured and predicted surface pressure distributions for front of train model.

Figure 11 displays the coefficient of pressure, Cp, corresponding to the surface pressures on the top(T_a, T_c) and sides(S_a, S_b) of the train body, versus the longitudinal length X. Here, T_a and T_c, refer to lines of intersection of the train top surface with the vertical planes Z=0 and Z=38, respectively. Whereas S_a and S_b refer to lines of intersection of the train side surfaces with vertical planes Z=48 and Z=51, respectively. The diagram displays simultaneously the values of the experimental values (C_p-Exp), and the corresponding predicted values from the seven models (Cp-RKE to C_p-SSTKW) .

The agreement between the results from the different models and measurements is seen to be very good on the top surface of the train; also the agreement between the results of the various models themselves, is near perfect in that region.

On the sides of the train, the agreement between the predicted results and measured ones is only fair, with the exception of the SA model which does much better, particularly at the plane S_a. It is expected that the flow on the sides of the train is much more complex due to the shedding of the leading edge vortices, and hence predicting it correctly is substantially more demanding from the turbulence models. However, it is surprising that the SA turbulence model, which is a one equation turbulence model, outperforms the 2-equation models, as well as the 7-equation Reynolds stress model.

The predicted values of the total drag coefficient are 0.375, 0.415, 0.363, 0.362, 0.386, 0.381, 0.357, for the SA, SKW, SSTKW, RSM, SKE, RNGKE, and RKE models, respectively. The corresponding measured value is 0.316.

SUMMARY AND CONCLUSION

Seven different models of turbulence were tested, ranging in complexity from the one equation SA model, up to the Reynolds Stress model. The results of predictions from all models were remarkably close. The agreement between them and measurements is generally very good, with the exception of the trailing edge region were the agreement is notably inferior. This is attributed to the flow over the train being highly streamlined and smooth for most of the domain, but also highly complex in some narrow regions depicting trailing edge vortices.

The agreement between the results of the different turbulence models is clearly better than between them and measurements, raising some questions regarding the extent to which the experimental conditions and the flow simulation specification coincide. Sources of discrepancy could be the assumed boundary conditions for k and ε , uniformity of the experimental conditions and interpolation errors in the predictions(particularly in the wall regions were high gradients are present). Experimental errors and interference effects by the measurement probe should also not be ruled out, particularly due to the small size of the model.

Comparison between predicted velocity and pressure values against their corresponding measured values, does not reveal a clear best performer among the turbulence models. Thus the recommended model for the high speed train application is the RKE model, since it is the closest in predicting the total drag force.

REFERENCES

King W.F. , Mackrodt P.A. and Pfizenmaier E. " The Aerodynamics and Acoustics of High-Speed Tracked Vehicles" Proc. Int. Conf. on Speedup Technology for Railway and Maglev Vehicles, B3-2-(3), Nov.22-26, 1993, Japan.

Mohamed,I.K., Experimental and Theoretical Investigation of the Flow Around High Speed Trains",PhD Thesis, Mechanical Engineering Department, Cairo University, 2006.

Bardina J.E., Huang P.G. and Coakley T.J. "Turbulence Modeling Validation, Testing and Development" NASA Technical Memorandum 110446, Performing Organization Report Number A-976276, April 1997

Launder,B.E. and Spalding,D.B. "The Numerical Computation of Turbulent Flows" Computer Methods in Applied Mechanics and Engineering,3,pp.269-289,1974.

Victor Yakhot and Steven A. Orszag "Renormalization Group Analysis of Turbulence: I. Basic Theory" Journal of Scientific Computing, Vol. 1, No. 1, 1986.

Victor Yakhot and Leslie M. Smith "The Renormalization Group, the ε-Expansion and Derivation of Turbulence Models" Journal of Scientific Computing, Vol. 7, No. 1, 1992.

Nagano Y. and Itazu Y. "Renormalization Group Theory for Turbulence: Assessment of the Yakhot-Orszag-Smith Theory" Fluid Dynamics Research 20,157-152, 1997.

Shish, T.H. ,Liou,W.W., Shabbir,A.,Yang,Z. and Zhu,J. "A New k-ε Eddy Viscosity Model for High Reynolds Number Flows-Model Development and Validation" Computers Fluids,24(3):227-238,1995.

Wilcox D.C. "Turbulence Modeling for CFD" DCW Industries Inc., La Canada California, 1998.

Menter F.R. "Two-Equation Eddy-Viscosity Turbulence Models for Engineering Applications" AIAA Journal, 32(8):1598-1605, August 1994.

Sarkar S. and Balakrishnan " Application of Reynolds-Stress Turbulence Model to the Compressible Shear Layer" ICASE Report 90-18, NASA CR 182002, 1990.

Gibson M.M. and Launder B.E. "Ground Effects on Pressure Fluctuations in the Atmospheric Boundary Layer" J. Fluid Mechanics, 86:491-511, 1978.

Launder B.E., Reece G.J. and Rodi W." Progress in the Development of a Reynolds Stress Turbulence Closure" J. Fluid Mechanics, 68(3):537-566, April 1975.

Brain E. Launder " Second-Moment Closure : Present and Future ?" Review, Int. J. Heat and Fluid Flow, Vol. 10, No. 4, Dec. 1989.

Kim S.E. and Choudhury D. "A Near-Wall Treatment Using Wall Functions Sensitized to Pressure Gradient" in ASME FED. Vol. 217, Separated and Complex Flows, ASME, 1995 cited in (30).

Versteeg H.K. and Malalasekera W. "An Introduction to Computational Fluid Dynamics; The Finite Volume Method" Textbook, Longman Group Ltd, 1995.